
Article:
Adeyemi, G.J., Dwyer-Joyce, R.S. orcid.org/0000-0001-8481-2708, Stephen, J.T. et al. (1 more author) (2019) Measurement of metal–roll interface during metal rolling using normal and oblique ultrasonic reflection. Tribology - Materials, Surfaces & Interfaces, 14 (2). pp. 79-91. ISSN 1751-5831

https://doi.org/10.1080/17515831.2019.1675338

Measurement of metal-Roll Interface During Metal Rolling Using Normal and Oblique Ultrasonic reflection

G. J. Adeyemi[1], R. S. Dwyer-Joyce[2], J. T. Stephen[1] and A. Adebayo[1]
[1] Department of Mechanical Engineering, Ekiti State University, Ado-Ekiti, Nigeria
[2] Department of Mechanical Engineering, The University of Sheffield, Mappin Street, Sheffield S1 3JD, UK.

Corresponding author:

Adeyemi, Gbenga Joshua
Department of Mechanical Engineering,
Ekiti State University, Ado-Ekiti, Nigeria
Email: adeyemi4unad@yahoo.com

Abstract

It is important to monitor the roll bite interface during metal rolling to maintain the product size and homogeneity so as to minimize the material wastage. However, the harsh nature of cold rolling makes installation of sensors in metal roll for industrial applications difficult. The present study used a novel ultrasonic measurement technique whereby an ultrasonic signal went through an external sensor layout arrangement to study the metal-roll interface. The reflection coefficient obtained from the roll-strip interface at 0^o to the roll surface (normal ultrasonic measurement technique) and 19^o (oblique ultrasonic measurement technique) were modelled and experimentally investigated on an instrumented pilot metal rolling mill. Variances of 6.4% and 8.8% were obtained in the reflection coefficient of the techniques from experimental and modelling approaches, respectively. This study showed the ability to use the normal and oblique ultrasonic reflections to study the effect of the angle of incidence wave on the reflection coefficient, and the reflection coefficient obtained from the metal-roll interface is only minimally affected by the incident angle not greater than 19^0.

Keywords
Ultrasound, cold rolling, strip thickness, roll-bite length, ultrasonic reflection, modelling

Nomenclature

τ	Shear stress, N/m^2
h	Oil thickness μm
μ	Coefficient of friction -
f	Ultrasonic frequency, MHz
R	Reflection coefficient
K	Stiffness, GPa/μm
K_L, K_S	Liquid and solid Stiffness, GPa/μm
u, w	Horizontal and vertical displacement, μm
ω	Angular frequency, rad/sec
Z	Acoustic impendence, kg/m^2s
β	Bulk of modulus, GPa

ρ Density, kg/m^3

C Speed of sound, m/Sec

A Amplitude of signal, mV

θ_i, θ_r Incidence and reflection angle, ^{0}

v Poisson's ratio

σ Stress , N/m^2

ε Strain , mμ

p_{nom} Normal contact pressure, Pa

k Wave number

1 INTRODUCTION

Metal rolling plays a significant role in the ever-growing modern manufacturing world [1]; the production of sheet metal from the slab is often done by metal rolling processes [2], and it involves interaction of machine components with the metallic material under load.

An understanding of the metal-roll interface conditions during the metal rolling process is very important in the metal forming process. This is for the proper monitoring of the metal roll and rolled strip surfaces as well as controlling of mechanical properties of the rolled strip during the rolling process [3]. The interface conditions to be controlled include the film thickness, roll stress, contact length and rolled strip thickness, which depend on the applied rolling load, speed and lubrication. However, there is a lack in the development of in-situ measurement techniques in metal rolling processes. The harsh nature of cold rolling makes instrumentation and implementing of in-situ sensors in industrial applications difficult.

Ultrasound is an attractive tool for non-invasive evaluation of the metal-roll interface conditions during metal rolling due to its high penetration power and sensitivity. Ultrasound pulse echo technique has been previously used to investigate metal- roll interface conditions during cold metal rolling process but with clear limitations [4-6]. In these studies, ultrasonic longitudinal and shear wave sensors were oppositely mounted on a plug pressurized in radial holes drilled in the roll and facing outwards from the roll. The reflection coefficient obtained from transmitted and reflected signals apparent to the roll bite was employed to calculate the actual rolled strip thickness during the rolling process.

However, any modification of the roll has the potential to negatively affect the manufactured strip. Thus, it is difficult to implement this technique in industrial setup due to the major roll modification involved, as well as the roll integrity at stake with the fatigue crack that can develop over time. Nevertheless, the studies have proven that ultrasonic method can be used to study metal-roll interface conditions during rolling operation.

As a result of the limitation of the pulse-echo technique, an external ultrasonic sensor arranged at angle technique (pitch-catch configuration as shown in Figure 4) is chosen as an alternative. The typical phenomenon of this technique is that the amplitude of the waveform of the obtained

reflected ultrasonic wave is dependent on the orientation of the sensor and the acoustic property of the material.

The ultrasonic measurement method is based on the propagation of sound signal produced by piezoelectric transducers. In the normal ultrasonic transmission method, measurement is made rapidly with high level of reliability and accuracy without damage to the transmission medium, and this technique can be used at different frequencies for measuring different thicknesses. Conversely, the use of ultrasonic oblique reflection method of measurement is quite challenging due to its layout arrangement [7].

Some researchers have used normal and oblique ultrasonic pulsing techniques to study solid-solid interface conditions, and compared the reflection coefficient obtained from the two techniques [7-12]. They mostly concluded that minor differences are observed in their reflection coefficient values, up to 22.5^0 of incidence angles. It could be deduced from the studies that the oblique reflection ultrasonic technique can also be applied in the determination of the roll interface conditions during the metal rolling process. Therefore, the aim of this paper is to build a measurement method for measuring roll interface conditions during the metal rolling process and model the physical mechanism.

2 THEORECTICAL APPROACH

When two rough surfaces are loaded, solid–solid contact is limited to the surface roughness/asperities junctions, with pockets of air at the void between the asperities. When ultrasonic longitudinal waves incident at the contact between the two solids, normal to the contact interface, part of the waves is transmitted at the asperity junctions whilst the remainder is reflected at the solid-air interface. The pockets of air around the asperities act as acoustic reflectors (as depicted in Figure 1a). The amount of sound transmitted depends on the wavelength of the sound wave relative to the air gap.

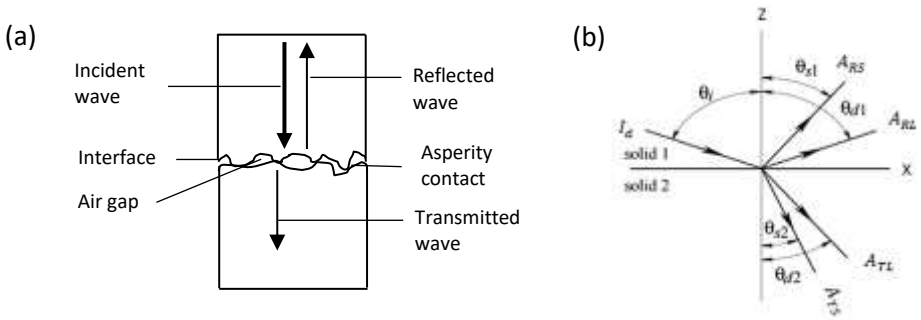

Figure 1: Ultrasonic reflection and transmission at rough solid-to-solid interface (a) normal incidence wave and (b) oblique incidence wave

If the incident waves are normal to a contact interface, the reflection coefficient, *R* which is the relative amplitude of the ultrasonic waves that is reflected, is given as:

$$R = \frac{z_1 - z_2}{z_1 + z_2} \qquad 1$$

where z_1 and z_2 are the acoustic impedance of the materials either side of the contact interface. When dry contact is loaded, the asperities deform and cause the area of contact to increase, and thus enabling a larger proportion of the incident ultrasound to be transmitted through to the interface. Kendall and Tabor [13] modelled the asperity interactions of the rough interface as a surface distributed spring system and found that the reflection coefficient depends on the interfacial stiffness, *K*. The interaction by an incident ultrasonic wave therefore results in a reflection coefficient governed by the relationship:

$$R = \frac{z_1 - z_2 + \frac{i\omega z_1 z_2}{K}}{z_1 + z_2 + \frac{i\omega z_1 z_2}{K}} \quad 2$$

where *K* is the equivalent spring stiffness and ω is the angular frequency of the ultrasonic wave. The stiffness, which is expressed per unit area, is defined as the change in nominal contact pressure, p_{nom}, required to cause unit approach of mean lines of the two surfaces. For a dry contact, *K* is governed by the normal stiffness of asperities alone, K_S, given as [14]:

$$K_S = \frac{dp_{nom}}{du} \quad 3$$

If a fluid is introduced into the interface, both the metal-to-metal asperity contact and the thin fluid film transmit a proportion of the incident ultrasonic energy. The liquid stiffness component, K_L which increases inversely with layer thickness of the liquid, acts in parallel to K_S and this is governed by the bulk modulus (*B*) and thickness (*h*) of the fluid as shown in Eq. (4) [15].

$$K_L = \frac{B}{h} \quad 4$$

Therefore, for a static lubricated rough surface contact, the total distributed stiffness, K, is given by the sum of the solid and liquid components. That is:

$$K = K_S + K_L \quad 5$$

The oblique transmission and reflection of longitudinal and shear incidence waves at a solid-solid interface is shown schematically in Figure 1b. I_d is longitudinal incidence wave and θ_i is the angle of incidence. A_{RL}, A_{RS}, A_{TL}, and A_{TS} are the reflected longitudinal, reflected shear, transmitted longitudinal and shear transmitted waves respectively, whileθ_{d1} andθ_{s1}, θ_{d2} and θ_{s2} are angles of reflection and transmission of each wave. When a longitudinal or shear ultrasonic wave hits the contact interface of the two media at any angle θ_i, mode conversion occurs at the boundary (reflection of incidence wave and refraction of the transmitted wave). Some portion of the wave is reflected at angle θ_{d1} the same as angle of incidence for the longitudinal wave, whilst the remainder of the wave that is transmitted into the second material refracted at the boundary and divided into two parts; longitudinal with an angle of θ_{d2} and shear with an angle of $\theta_{s2.}$ The angles of reflection and refraction of the transmitted waves depend on the acoustic properties of the materials, the angle of incidence and the nature of the interface.

The reflection and refraction of ultrasound waves at the boundary of two media is governed by Snell's law. Therefore, when the incidence angle and speed of sound in the materials are known, the angles of reflection and refraction of the transmitted signals at the boundary of these materials can

be determined [12]. The relationship between the incidence and reflected angles at the materials interface shown Figure 1b is expressed by:

$$\frac{\sin\theta_i}{c_{Id}} = \frac{\sin\theta_{dI}}{c_{RL}} = \frac{\sin\theta_{sI}}{c_{RS}} = \frac{\sin\theta_{d2}}{c_{TL}} = \frac{\sin\theta_{s2}}{c_{TS}} \quad 6$$

where θ_i is angle of incidence, θ and c are the angle and speed of sound, respectively, and the subscripts are as earlier defined for the different waves. The relationship between speed of sound c and wave-number, k, is expressed as follows:

$$c = \frac{\omega}{k} \quad 7$$

where ω is the angular frequency of the sound wave. Substituting Equation 7 into Equation 6 gives:

$$k_{Id}\sin\theta_i = k_{RL}\sin\theta_{dI} = k_{RS}\sin\theta_{sI} = k_{TL}\sin\theta_{d2} = k_{TS}\sin\theta_{s2} \quad 8$$

2.1 Propagation of the Oblique Incidence Wave through an Embedded Layer

Figure 2 shows the characteristics of the reflection and transmission of an oblique longitudinal incidence wave at a thin layer of fluid. The layer is considered as a microscopic interface with effective properties dependent on the interface structure [16]. The angles of reflection and transmission indicated are derived from equation 6. Their relationship is shown in Equation 8.

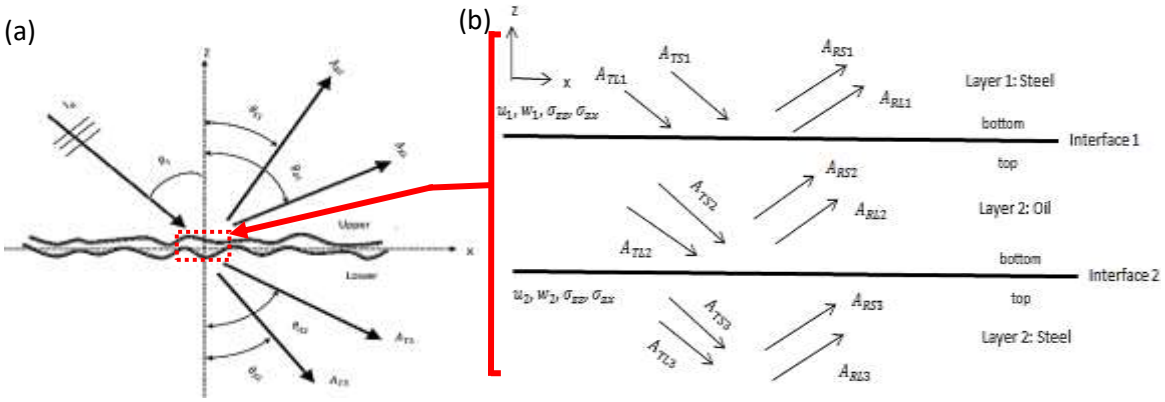

Figure 0: (a) Transmission of an incidence longitudinal wave [12] and (b) Mode conversion and interaction of signal within the embedded layer

In Figure 2, the interface between the two solid media is considered as a single layer. The particle velocities (or displacements) and stresses on the upper and lower interfaces between the layer can be related to each other with the aid of a transfer matrix expressed as follows [7]:

$$\begin{Bmatrix} \sigma_{zz} \\ \sigma_{zx} \\ w \\ u \end{Bmatrix}_t = [M] \begin{Bmatrix} \sigma_{zz} \\ \sigma_{zx} \\ w \\ u \end{Bmatrix}_b \quad 9$$

where $[M]$ is 4×4 matrix, the subscripts b and t denote the bottom and top layers, while σ_{zz} and σ_{zx} are the normal and tangential stresses. Also, w and u are the vertical and horizontal displacements. The elements of the matrix M depend on the layer property. Equation 9 can be regarded as the

boundary condition, which relates the stress and particle displacement between the top and the bottom layered interfaces.

Once the longitudinal wave strikes interface 1 (bottom of layer 1) at an angle, the transmitted and reflected waves produce a unique stress and displacement on both sides of the layer [17]. The amplitudes of the reflected and transmitted waves may be found by using the matrix Equation 9. The deflections of the longitudinal and shear wave are given by Pilarski *et al.* [9] :

For the horizontal displacement:

$$u_L{}^+ = A_L{}^+ \sin\theta_{d2} e^{(ik^L \cos\theta_{d2} Z)} \quad 10$$

$$u_T{}^+ = -A_T{}^+ \cos\theta_{s2} e^{(ik^S \cos\theta_{s2} Z)} \quad 11$$

$$u_L{}^- = A_L{}^- \sin\theta_{d1} e^{(-ik^L \cos\theta_{d1} Z)} \quad 12$$

$$u_T{}^- = A_T{}^- \cos\theta_{s1} e^{(-ik^S \cos\theta_{s1} Z)} \quad 13$$

For the vertical displacement:

$$w_L{}^+ = A_L{}^+ \cos\theta_{d2} e^{(ik^L \cos\theta_{d2} Z)} \quad 14$$

$$w_T{}^+ = A_T{}^+ \sin\theta_{s2} e^{(ik^S \cos\theta_{s2} Z)} \quad 15$$

$$w_L{}^- = -A_L{}^- \cos\theta_{d1} e^{(-ik^L \cos\theta_{s1} Z)} \quad 16$$

$$w_T{}^- = A_T{}^- \sin\theta_{s1} e^{(-ik^S \cos\theta_{d1} Z)} \quad 17$$

The u_L and w_L in the *x* and *z* axes are the displacement vectors of the longitudinal (shear) waves in the upper and lower parts of the layer boundaries. The values of u_L and $u_T$were set to zero, because the structure is assumed to be in two dimensions and the y coordinate axis is implicit and is omitted in the mathematical expression. The superscripts (+) and (-) indicate the up and down movements of the wave at the layer interface respectively. While z is distance in the direction of wave propagation and A_L and A_T are the amplitudes of the displacement waves. In addition, k^L and k^S are longitudinal and shear wave numbers and expressed as follows:

$$k^L = \frac{\omega}{C_L} \text{ and } k^S = \frac{\omega}{C_S} \quad 18$$

while c_L and c_S are the velocities of longitudinal and shear waves in the infinite isotropic medium. Normal and tangential stresses can be determined at any point within the isotropic and homogeneous boundary layers with the stress and strain relations:

$$\sigma_{ij} = \Lambda_{ij}\varepsilon_{kk} + 2\mu\varepsilon_{ij} \quad 19$$

The relationships between the Lame constants$(\Lambda + \mu)$, density and velocities of longitudinal and shear waves shown in Equations 18 and 19 can used to calculate the stresses and displacement components in both *x* and *z* axes respectively. The relationships are expressed by:

$$\sigma_{xx} = \Lambda\frac{\partial u_z}{\partial z} + (\Lambda + 2\mu)\frac{\partial u_x}{\partial x} \quad 20$$

and

$$\sigma_{zx} = \mu(\frac{\partial u_x}{\partial z} + \frac{\partial u_z}{\partial x}) \quad 21$$

while

$$\mu = \rho {c_S}^2 \quad (22)$$

and

$$\lambda + 2\mu = \rho {c_L}^2 \quad (23)$$

The normal and tangential stresses and displacements at the material boundaries can be determined by the relationships 10 to 23.

As previously explained, the oblique longitudinal or shear wave reflection coefficient at an interface can be obtained with a transfer matrix approach [7, 10]. This can be done by relating the stresses and displacement components at the top face with those at the bottom. The bottom layer is denoted as *k* while the top layer is denoted as *k*+1. For the boundary conditions, the continuity of normal and tangential stresses and displacements between the top and bottom faces are satisfied and expressed by the following matrix equation:

$$[M_{k,b}] \begin{Bmatrix} A_{RL,k} \\ A_{RS,k} \\ A_{TL,k} \\ A_{TS,k} \end{Bmatrix} = \begin{Bmatrix} \sigma_{zz} \\ \sigma_{zx} \\ w \\ u \end{Bmatrix}_b \quad (24)$$

$$[M_{k+1,t}] \begin{Bmatrix} A_{RL,k+1} \\ A_{RS,k+1} \\ A_{TL,k+1} \\ A_{TS,k+1} \end{Bmatrix} = \begin{Bmatrix} \sigma_{zz} \\ \sigma_{zx} \\ w \\ u \end{Bmatrix}_t \quad (25)$$

$$[M_{k,b}] \begin{Bmatrix} A_{RL,k} \\ A_{RS,k} \\ A_{TL,k} \\ A_{TS,k} \end{Bmatrix} = \begin{Bmatrix} \sigma_{zz} \\ \sigma_{zx} \\ w \\ u \end{Bmatrix}_b = [M_{k+1,t}] \begin{Bmatrix} A_{RL,k+1} \\ A_{RS,k+1} \\ A_{TL,k+1} \\ A_{TS,k+1} \end{Bmatrix} = \begin{Bmatrix} \sigma_{zz} \\ \sigma_{zx} \\ w \\ u \end{Bmatrix}_t \quad (26)$$

For the solid-oil-solid system, equation 26 is chosen according to the generalised multi-layered system. Therefore, the relationship of interface 1 and interface 2 in Figure 2 is expressed as follows:

$$[M_{1,b}]\begin{Bmatrix}A_{RL,1}\\A_{RS,1}\\A_{TL,1}\\A_{TS,1}\end{Bmatrix}=[M_{2,t}]\begin{Bmatrix}A_{RL,2}\\A_{RS,2}\\A_{TL,2}\\A_{TS,2}\end{Bmatrix} \quad 27$$

$$[M_{2,b}]\begin{Bmatrix}A_{RL,2}\\A_{RS,2}\\A_{TL,2}\\A_{TS,2}\end{Bmatrix}=[M_{3,t}]\begin{Bmatrix}A_{RL,3}\\A_{RS,3}\\A_{TL,3}\\A_{TS,3}\end{Bmatrix} \quad 28$$

The problem is solved by assembling equations 27 and 28 to give:

$$\begin{bmatrix}[M_{1,b}] & -[M_{2,t}] & [0]\\ [0] & [M_{2,t}] & [M_{3,t}]\end{bmatrix}\begin{Bmatrix}A_{RL1}\\A_{RS1}\\A_{TL1}\\A_{TS1}\\A_{RL2}\\A_{RS2}\\A_{TL2}\\A_{TS2}\\A_{RL3}\\A_{RS3}\\A_{TL3}\\A_{TS3}\end{Bmatrix}=\{0\} \quad 29$$

In summary, four waves, longitudinal transmission, longitudinal reflection, shear transmission and shear reflection are considered in each medium (Figure 2). The boundary displacements and stresses of each layer are expressed in the form of matrix equations. These boundary conditions are satisfied by equating two sets of matrix equations involving displacements and stresses. The final equation to obtain the reflection coefficient is expressed as follows:

$$[M_b]\{X\} = [M_t]\{Y\} \quad 30$$

$$\{X\} = [M_b]^{-1}[M_t]\{Y\} \quad 31$$

In Equation 31, M_i generally explained the relationship between the amplitudes of the normal and shear stresses and displacement at any location on the media. As explained by Liaptsis *et al.* [11], the amplitude of the incident longitudinal and shear waves in layer 1 will be equal to zero because the input wave was from layer 2.

Once the material properties and the incidence angle are known, the reflection coefficient is solved by the matrix equations shown in 27 and 28. Since the amplitude value of the incident wave is 1, the elements in the vector $\{X\}$ are the reflection coefficients to be found.

$$[M_b] = \begin{bmatrix} i\omega\rho_1\alpha_1\psi_1/g_{l1} & 2i\omega\rho_1 s{\beta_1}^2\xi_1/g_{s1} & -i\omega\rho_2\alpha_2\psi_2/g_{l2} & 2i\omega\rho_2 s{\beta_2}^2\xi_2/g_{s2} \\ -2i\omega\rho_1 s{\beta_1}^2\gamma_1/g_{l1} & i\omega\rho_1{\beta_1}^2\psi_1/g_{s1} & -2i\omega\rho_2 s{\beta_2}^2\gamma_2/g_{l2} & -i\omega\rho_2{\beta_2}^2\psi_2/g_{s2} \\ \alpha_1 s/g_{l1} & -\xi_1/g_{s1} & -\alpha_2 s g_{l2} & -\xi_2 g_{s2} \\ -\gamma_1/g_{l1} & -\beta_1 s/g_{s1} & -\gamma_2 g_{l2} & \beta_2 s g_{s2} \end{bmatrix} \quad 32$$

$$[M_t] = \begin{bmatrix} i\omega\rho_2\alpha_2\psi_2/g_{l2} & 2i\omega\rho_2 s{\beta_2}^2\xi_2/g_{s2} & -i\omega\rho_1\alpha_1\psi_1/g_{l1} & 2i\omega\rho_1 s{\beta_1}^2\xi_1/g_{s1} \\ -2i\omega\rho_2 s{\beta_2}^2\gamma_2/g_{l2} & i\omega\rho_2{\beta_2}^2\psi_2/g_{s2} & -2i\omega\rho_1 s{\beta_1}^2\gamma_1/g_{l1} & -i\omega\rho_1{\beta_1}^2\psi_1/g_{s1} \\ \alpha_2 s/g_{l2} & -\xi_2/g_{s2} & -\alpha_1 s g_{l1} & -\xi_1 g_{s1} \\ -\gamma_2/g_{l2} & -\beta_2 s/g_{s2} & -\gamma_1 g_{l1} & \beta_1 s g_{s1} \end{bmatrix} \quad 33$$

Vector $\{Y\} = \begin{Bmatrix} 0 \\ 0 \\ 1 \\ 0 \end{Bmatrix}$ for longitudinal incident wave.

While the matrix symbol parameters are defined as follows:

$$s = \frac{\sin\theta_{IL}}{\alpha} = \frac{\sin\theta_{IS}}{\beta} \quad 34$$

$$\gamma = \sqrt{1 - \alpha^2 S^2} \quad 35$$

$$\xi = \sqrt{1 - \beta^2 S^2} \quad 36$$

$$\psi = 1 - 2\beta^2 S^2 \quad 37$$

$$g_l = exp\left(\frac{i\omega\gamma y}{\alpha}\right) \quad 38$$

$$g_s = exp\left(\frac{i\omega\xi y}{\beta}\right) \quad 39$$

Matrices $[M_b]$ and $[M_t]$ are employed in equations 32 and 33 to determine the reflection coefficient matrices $\{X\}$.

2.2 Modelling the Steel-Oil-Steel Interface

To study the effect of the incident angles in ultrasound wave propagation at the interface of a metal roll and strip, computer simulations of the reflection coefficient of the incident wave were conducted at two different loads with the pulse-echo and pitch-catch ultrasonic transmission techniques.

The interface between two solids with a thin layer of another material in-between has a significant effect on the wave reflection and mechanical behaviour of the interface [9]. A solid-oil-solid interface could be classified as rigid and slip interfaces, depending on the thickness of layer of the interface [18]. Slip interface in solid-oil-solid can be achieved if the interface layer is a thin ideal liquid with the thickness of the layer significantly large enough to separate the interface. However, mixed contact interface is considered in this study with the thin lubricant layer not sufficient to separate the media interface and consequently, the interface consists of isolated asperity contacts surrounded by the gaps filled with liquid.

A model developed by Pialucha [16] to evaluate the ultrasonic oblique reflection coefficient incidence for non-destructive characterization of the adherent/adhesive interface of bonded joints was considered for the present study due to its suitability to the present research. An adhesive layer between two solids was considered in his study while an oil layer is considered in the present study.

2.2.1 Modelling Procedure

Embedded oil film thickness 2.32 μm and 1.27 μm were used under the rolling loads of 60 kN and 90 kN with the 26 mm/sec roll speed. Also, frequencies of 0 to 10 MHz were used and the modelling was carried out with the solid-oil-solid interface. The ultrasonic sensor was mounted at an inclined angle, operating in a pitch-catch orientation (Figure 4). The simulations were run for longitudinal waves between the incidence angles of 0^o and 19^o. The reflection coefficients of the signals obtained from the modelling were stored for further studies. The analysis (Equations 32 and 33) of the whole process was conducted using script written in MATLAB.

3 EXPERIMENTAL APPROACH

3.1 Pilot Roll Mill

The pilot mill employed in this metal rolling experiment is a two roll mill type, with the upper and lower cylindrical rolls of diameter 110 mm each rotating in opposite directions (Figure 3). The pilot mill has a maximum roll gap of 5 mm roll width of 50 mm, contact length of 5 mm, load capacity of 250 kN and rolling speed of 26 mm/s. The average surface roughness of the roll was measured as Rq = 0.7 µm and the surface hardness of the metal roll was measured as 750 HV. Two load cells mounted between the upper roll machine frame of the machine to measure the rolling force. The machine permits both dynamic and stationary operating conditions

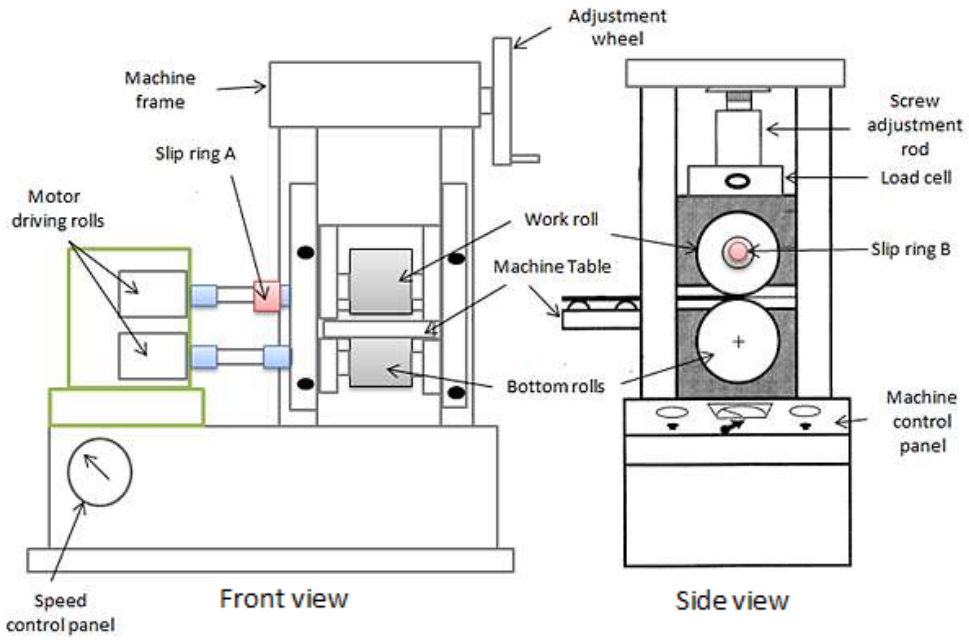

Figure 3: Sketch of the pilot mill employed

3.2 Roll Instrumentation

Figure 4 shows the schematic layout of an instrumented roll. The roll was instrumented with 10 MHz and 5 MHz central frequencies of longitudinal and shear sensors, respectively, mounted centrally and at both edges of the roll for transmission of signal. Four sensors (two longitudinal and two shear) were mounted on both sides of the upper roll at angle of incidence θ_i. The first pair of sensors (longitudinal and shear) on the right side act as pulsers and generate ultrasonic signals that were transmitted to the metal-roll interface, whilst the other pair of sensors (longitudinal and shear) on the left side of the roll act as receivers of the reflected signal from the metal-roll interface during the operation. The remaining two sensors (shear and longitudinal) were arranged on the top surface of the roll for the normal ultrasonic transmission (pulse–echo technique).

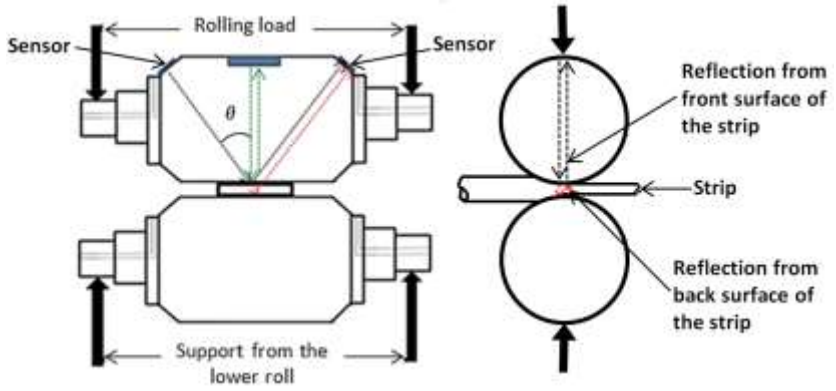

Figure 4: Rolls and sensors layout

3.3 Test Procedure

The experiment was conducted using a 5 mm thick, 25 mm wide and 250 mm length of strip (steel grade EN24). The strip was manually loaded between the rolls of the pilot rolling machine (Figure 5) after the lubricant had been applied to the surface of the strip. Loads of 70 kN and 90 kN were applied during the rolling operations. During the rolling process, ultrasonic signals were sent through the roll to the metal-roll interface and the reflected ultrasonic signals were continuously captured as the roll rotates as the strip passes through. The reflected signals were captured and digitized, and streamed directly to the hard disk of the computer for further processing and analyses.

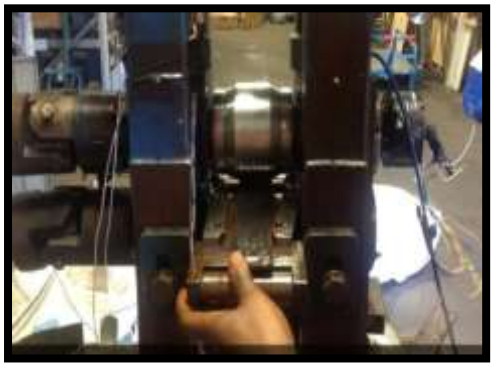

Figure 5: Feeding of the strip into the pilot rolling mill

3.4 Signal Processing

The raw reflected data (Figure 6(a)) obtained during the rolling operation contained both reference and reflected wave data at both roll-air and roll-strip contact interfaces, respectively. The reference data (total wave reflection) were obtained when the sensor was out of focus on the metal-roll interface (i.e. roll bite) while the reflected data (partial wave reflection) were obtained when the sensor focused on the metal-strip interface. Therefore, to permit meaningful analysis of the results, the data set was filtered to obtain extracted reflected data (reference and reflected signal) as shown in Figure (Figure 6(b)). Thereafter, the aquired signals were processed in the frequency domain in terms of amplitude values for both reference and reflected signals (Figure 6(c)).

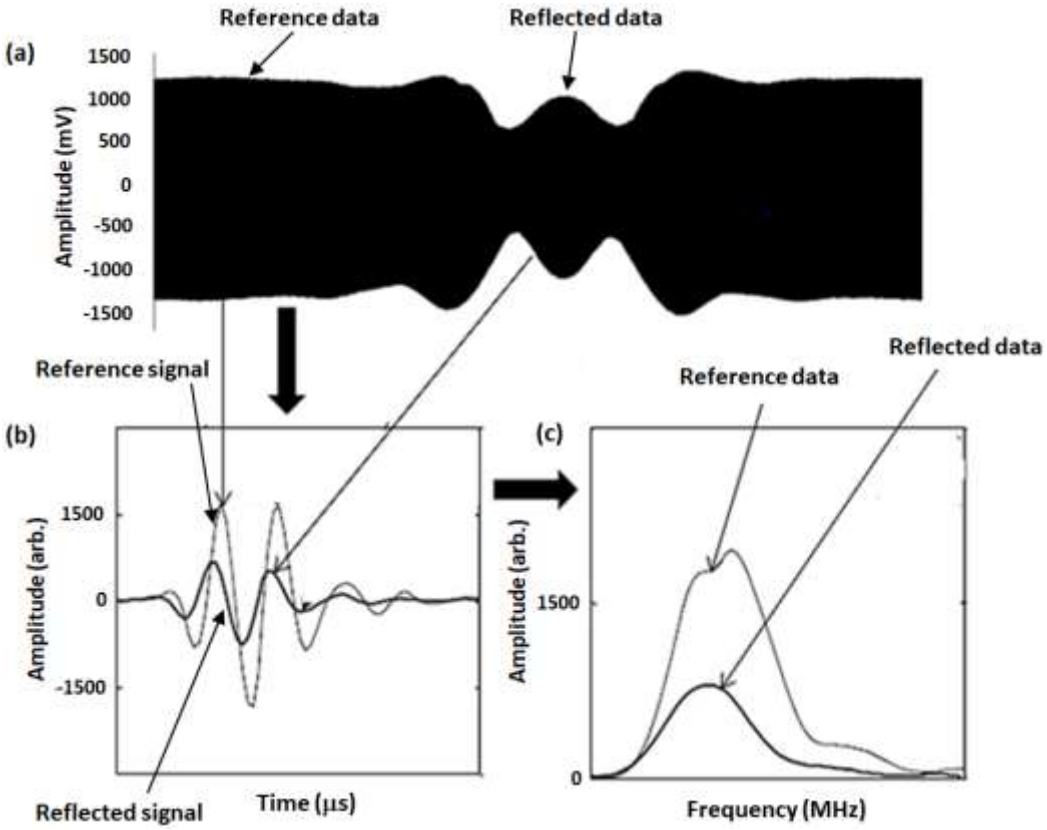

Figure 6: Processed reflected signal obtained from metal-roll interface d uring the rolling operation (a) stream of raw reflected data (b) extracted ultrasonic data in time domain (c) extracted ultrasonic data in frequency domain

4 RESULTS AND DISCUSSION

4.1 Modelling Results

Figure 7 shows the reflection coefficient at 0^o (pulse-echo ultrasonic technique) and 19^o (pitch-catch oblique ultrasonic technique) angles of incidence under the variable values of the oil film thicknesses as a function of frequency. From the figure, 0^o angle of incidence has the maximum values of 0.9 and 0.81 as the reflection coefficient. Small changes of approximately 0.08 reflection coefficient value were observed in the results as the angle of incidence increased from 0^o to 19^o for both film thicknesses of embedded layer respectively.

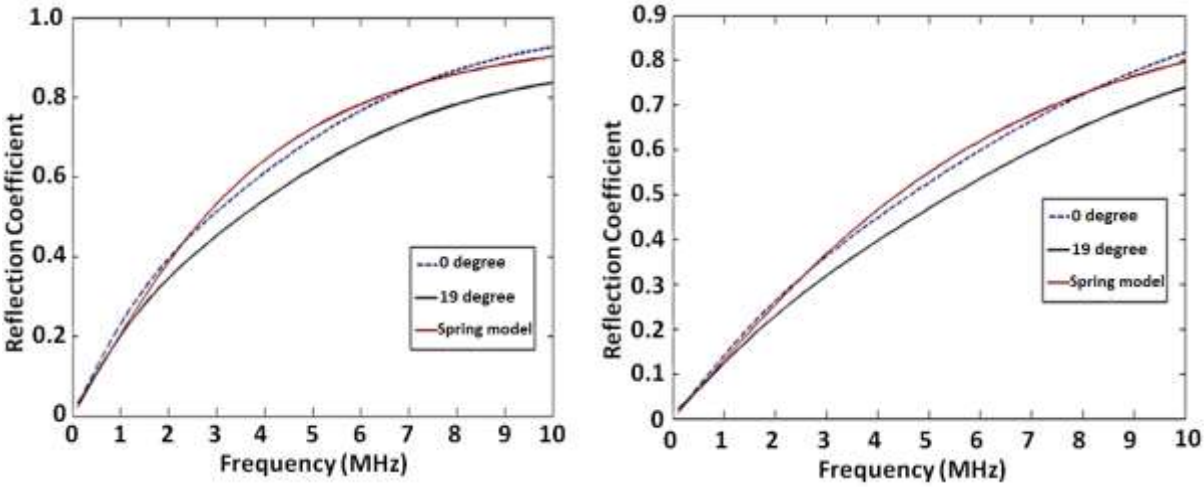

Figure 7: Reflection coefficients obtained from modelling under (a) 2.32 μm oil film thickness and (b) 1.27 µm oil film thickness

In addition, in order to check if the modelling conformed within the spring model regime, the oil film thicknesses applied during the modelling was used to determine the surface stiffness using the bulk modulus property of the oil as expressed in Equation 4. The stiffness values obtained were used in the spring model (Equation 5) to determine the reflection coefficient values for the frequency range 0 to 10 MHz. The resulted values reflection coefficient for the applied oil film thicknesses applied were plotted against the frequency as shown in Figure 7. As it can be observed from the figure, the values reflection coefficient obtained from modelling in normal pulsing technique (0^o angle of incidence) and the values reflection coefficient obtained using the spring model were 95% equal for the range of frequency studied.

Furthermore, Figure 8 illustrates the relationship between the changes in reflection coefficient with angle of incidence wave (obtained at 10 MHz of 0 degree and 19 degree of angles of incidence) in respect to the oil film thicknesses. As can be seen, oil film thickness has only a minor effect on ratio of the reflection coefficient value to changes to the angles of incidence. The constant ratio of $\frac{R0}{R19}$ regardless of the film thickness implies that no adjustment needs to be made for different film thickness, and this makes practical implementation easier.

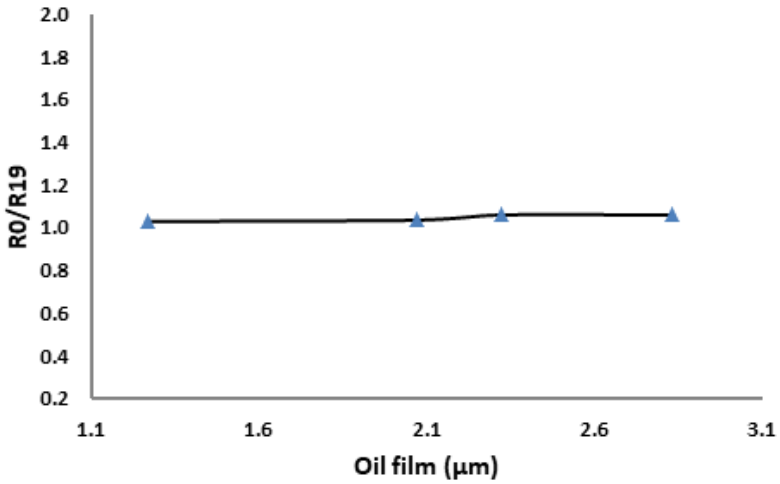

Figure 8: Change in reflection coefficient with angles against the oil film thicknesses

4.2 Experimental Results

Reflection coefficient of the wave reflected from the metal-roll interface was obtained by dividing the reflected peak amplitude value with the reference peak amplitude value. This reflection coefficient value was used further to calculate the stiffness value at the metal-roll interface during the rolling process.

The various reflection coefficients obtained along the roll-bite with time-of-flight (time domain) are shown in Figure 9. On the left and right parts of the curve, the reflection coefficient values are close to 1 which means that most of the incident ultrasonic signal is reflected and captured by sensor (receiver). At this part, the sensor was out of focus on the metal-roll interface (i.e. roll bite). At points A and B (before the entry and after the exit of the roll bite, respectively), the reflection coefficient is great than 1. These high values of reflection coefficient might be due to interference at these points, and this was also observed by Carreta *et al*. [5]. The value of reflection coefficient decrease within the roll bite, and this can be attributed to the decrease in reflected ultrasonic signal as sensor beam now focused on the roll bite (metal-strip interface). The centre value of this figure was used as the reflection coefficient of the reflected signal obtained from the metal-roll interface.

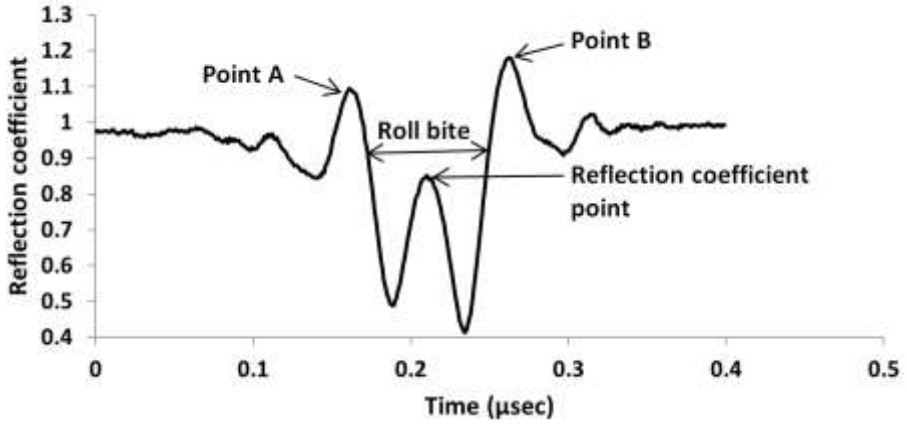

Figure 9: Longitudinal signal transmission at strip-to-roll interface during the rolling process

The data obtained under the applied rolling loads from normal and oblique ultrasonic reflection are presented in Figures 10. These data were obtained from the processed raw data presented in Figure 6. The figure (Figure 10) shows decreases in the amplitude of the reflected signal as the applied load increases for both techniques.

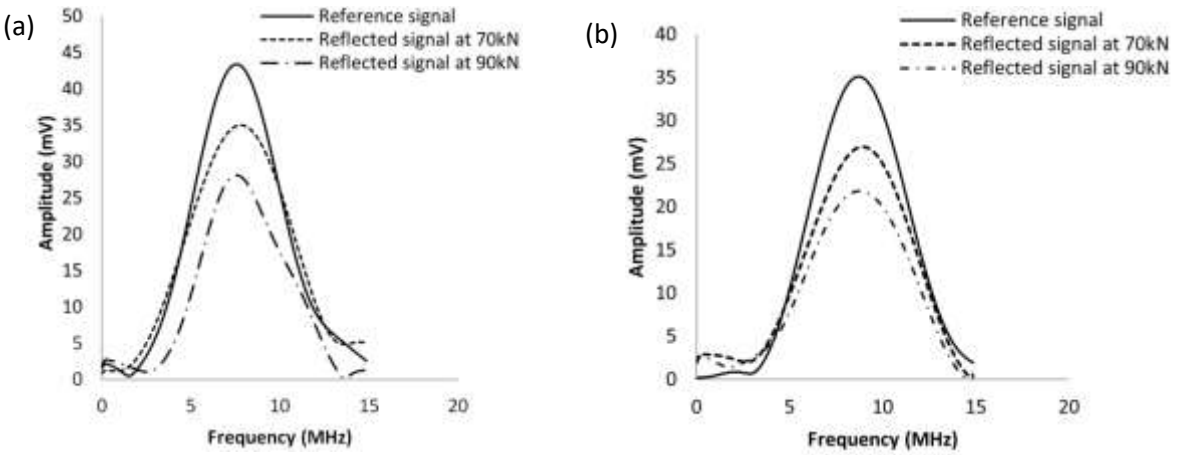

Figure 10: Wave amplitude spectrum of the (a) pulse-echo and (b) pitch-catch values as load is increased

Figure 11 shows reflection coefficient against frequency results, for frequencies lying within the bandwidth of each reference spectrum (4–10 MHz), from both techniques during the metal rolling process. As it can be observed in Figure 11(a), the experimental reflection coefficients across the bandwidth of the sensor through the pulse-echo technique were observed to be frequency dependent. The reflection coefficient from the metal-roll interface was found to increase as the frequency increases for both applied rolling loads.

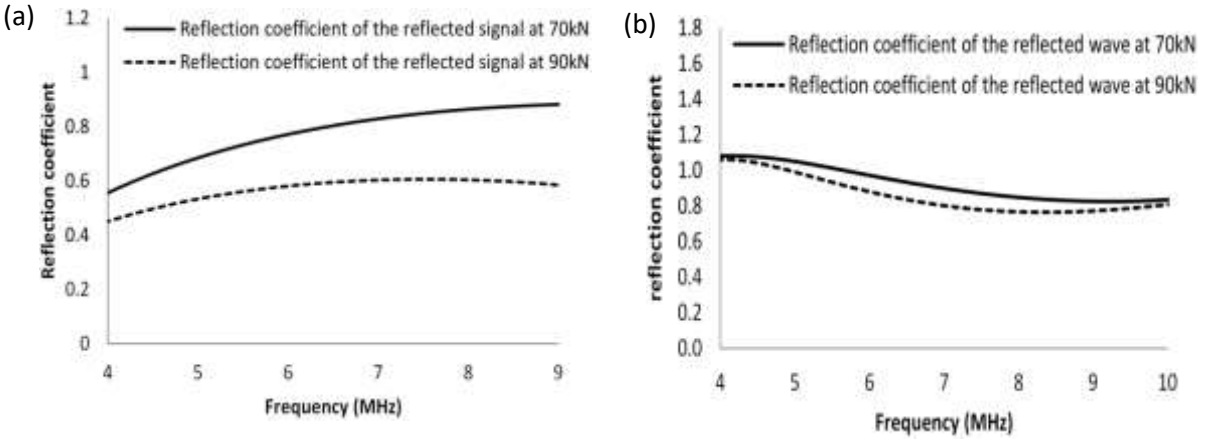

Figure 11: Longitudinal reflection coefficient against the frequencies with (a) pulse-echo technique and (b) pitch-catch technique

Figure 11(b) shows the variation of the experimental longitudinal reflection coefficient with frequency for 70 kN and 90 kN applied rolling loads. The reflection coefficient appears to decrease over the bandwidth of the sensor, which is a poor agreement with the spring model predictions in Figures 7. The disagreement which is consistent and could be seen across all results is attributed to the fact that the spring model is only for normal incidence/reflection. Liaptsis *et al.* [11] explained that this poor agreement was due to the increase of the angle orientation of the sensor that leads to the divergent beam in the steel that can result in reflection from more than the centre region of the interface contact.

The experimental reflection coefficient values obtained were used to calculate the interface stiffness values for both techniques (pitch-catch and pulse-echo), and consequently, the results were used to

determine the oil film thicknesses formed. The oil film thickness values obtained were then utilised to model layer's thickness between the two surfaces to obtain the model reflection coefficient values as illustrated in Figure 12.

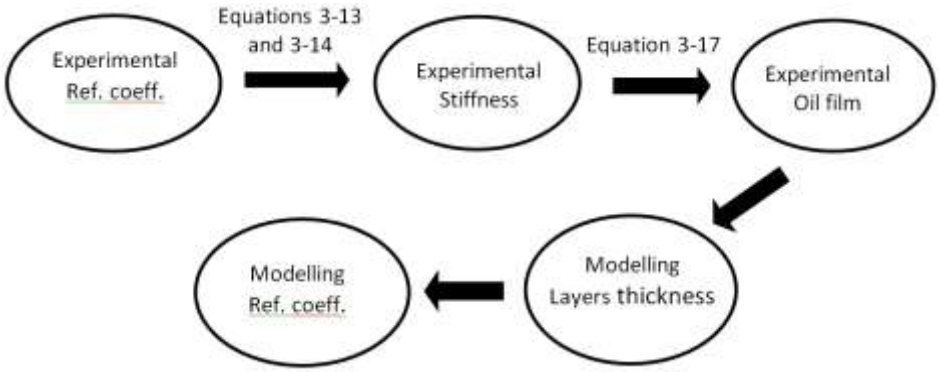

Figure 12: Flow chart of showing the steps for comparing experimental and predicted.

The obtained reflection coefficients from the normal and oblique ultrasonic reflection under the modelling and experimental procedure are shown in Figure 13. These were calculated from the ratio of the reflected amplitude value to the reference amplitude value using Equation 2. The reflection coefficients from both techniques were found to decrease as the applied load increases.

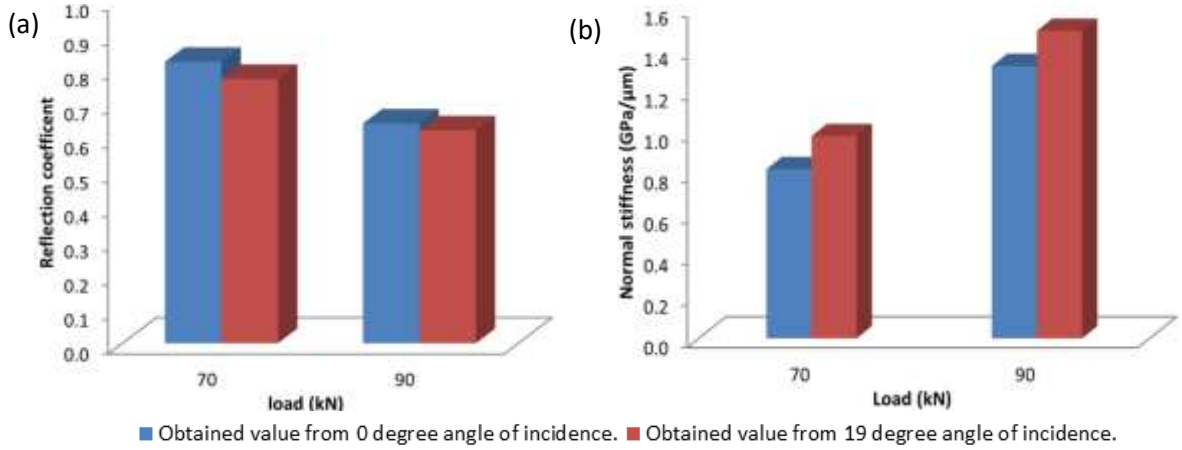

Figure 13: (a) Reflection coefficient and (b) Stiffness obtained from both techniques

However, the calculated values of normal stiffness using the obtained values of the reflection coefficients increased from 0.82 GPa/µm to 0.77 GPa/µm, and .82 GPa/µm to 0.98 GPa/µm for 0^{o} and 19^{o} incidence angle, respectively.

Figure 14 shows the reflection coefficient values obtained using spring model equation (Equation 5) against frequency as the stiffness of the interface at the different angles of incidence used under the two applied load during the metal rolling process. As can be seen from the figure, the higher stiffness values are recorded from the 19^{o} angle of incidence for both loads which shows that the angle of incidence has some degree of effect on the experimental stiffness value obtained from steel-oil-steel interface. This can be attributed to the double effect (reflection) expressed on reflection coefficient value of the spring model used to calculate the stiffness from the oblique approach.

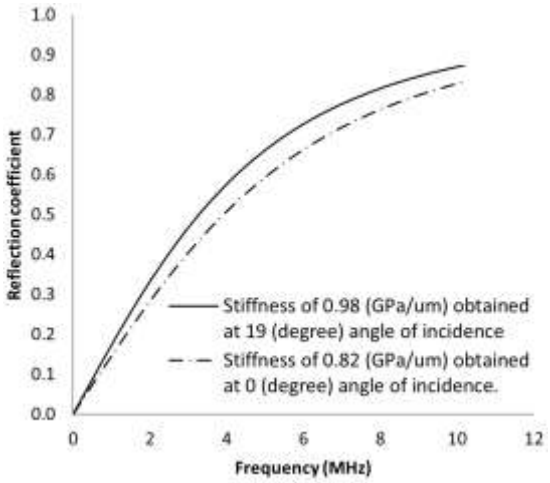

Figure 14: Reflection coefficient against frequency with stiffness values under 70 kN load

The spring model is normally used to authenticate for the normal pulsing technique, however, it was used to calculate the stiffness from the data obtained by the pitch-catch technique in the current study. This was due to the small variation observed in the reflection coefficients of sound waves between the 0^{o} and 19^{o} angles of incidence, and also, oblique reflection ultrasonic transmission techniques have been proven as best way to study the sensitivity of interface of the two materials with low frequency and the appropriate angle of incidence sound wave [8, 9, 19]. Therefore, the difference in the stiffness observed between the two configurations under the applied rolling loads is negligible and proved to be within the expected range of error.

4.3 Comparison of Experimental Results with Model Results

Figure 15 shows the comparison between the reflection coefficients of the incident wave obtained from the experiments and the modelling for normal pulsing (pulse-echo measurement) and oblique reflection (pitch-catch measurement) techniques with 2.32 μm and 1.27 μm oil film thickness embedded layer.

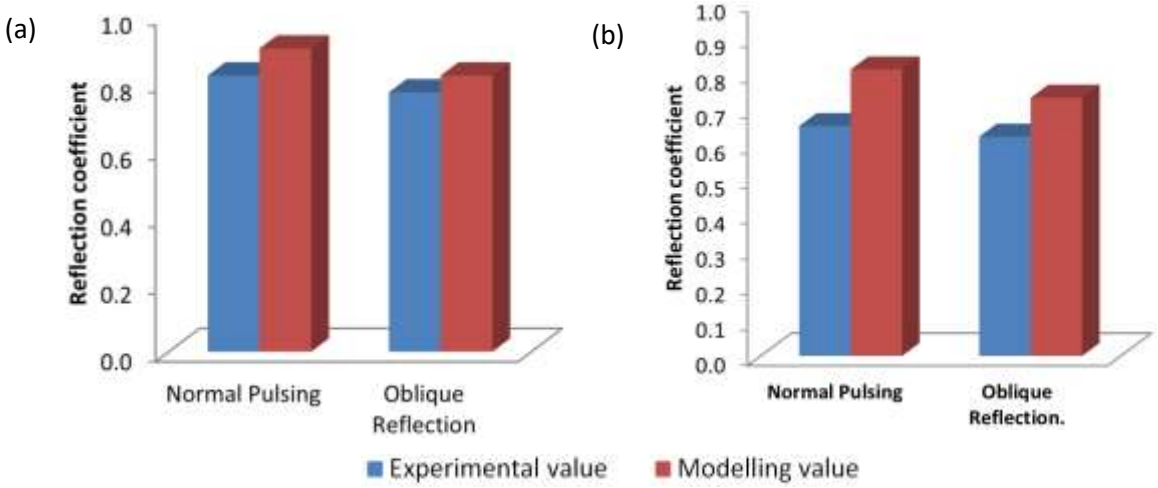

Figure 15: Reflection coefficient values obtained from modelling under (a) 2.32 μm and (b) 1.27 μm oil film thicknesses

As it can be seen from the figure, the higher values of the reflection coefficients were obtained from the modelling process and decrease as the oil film thickness (embedded layer) decreases. The reflection coefficient value obtained from normal and oblique ultrasonic transmission methods are slightly different from each other with 6.5% while for the model approach a different of 8.8% was recorded. This can be attributed to the formation of more asperity contacts at the metal-roll interface as a result of reduction of the embedded layer (oil film thickness). It promotes more transmission of ultrasonic signal, a reduction in the amplitude of the reflected wave and consequently, reduction in the value of reflection coefficient obtained during the rolling process. However, the difference in the reflection coefficients between the two measurement techniques employed is negligible. Furthermore, the reflection coefficients obtained from the processes show the same trend, they decreased as the value of the embedded layer of the interface decreases.

The percentage difference in the reflection coefficients from both processes (both modelling and experimental) for the applied different measurement techniques were determined by relating the reflection coefficients as shown in the expression:

5 CONCLUSION

A novel ultrasonic measurement technique whereby an ultrasonic signal went through an external sensor layout arrangement to study the metal-roll interface conditions during the metal rolling process. Experimental tests were carried out using normal and oblique measurement techniques under embedded oil thickness layer. Simulations were conducted using a model approach of Pialucha [16] for the embedded interface case to study the effect of the incidence angle on the longitudinal wave reflection coefficient. The following can be concluded:

- This study has shown the ability to use the normal and oblique ultrasonic reflections to study the effect of the angle of incidence wave on the reflection coefficient;
- The reflection coefficient value obtained from normal (0^0) and oblique (19^0)ultrasonic transmission methods are slightly different (6.5% for experimental values), which shows that the oblique arrangement could be used to study roll-strip interface during rolling operation using spring model;
- The stiffness value obtained from both normal and oblique ultrasonic transmission techniques is a little different of 16% (at 70 kN) and 7% (at 90 kN) from each other due to increase asperity contact at the interface as the load increases. As load increases, different in stiffness value between the measurement techniques reduces;
- This study has proven that the reflection coefficient obtained from the interface layers is only minimally affected by the incident angle not greater than 19^0 investigated in this study.

Reference

1. Roberts, W.L., *Cold rolling of steel*. 1978, New York: McGraw Dekker.
2. Schey, J.A., *Metal Deformation Processes/Friction and Lubrication*. 1970: IL Iit Reseach Inst. Chicago.

3. Garcia, D.F., M. Garcia, F. Obeso, and V. Fernandez, *Flatness measurement system based on a nonlinear optical triangulation technique.* IEEE Transactions on Instrumentation and Measurement, 2002. **51**(2): p. 188-195.
4. Dwyer-Joyce, R. and A. Hunter. *A novel sensor for lubrication and contact measurement in metal rolling*. in *5th World Tribology Congress, WTC 2013*. 2013: Politecnico di Torino (DIMEAS).
5. Carretta, Y., A. Hunter, R. Boman, J.-P. Ponthot, N. Legrand, M. Laugier, and R. Dwyer-Joyce, *Ultrasonic roll bite measurements in cold rolling – Roll stress and deformation.* Journal of Materials Processing Technology, 2017. **249**: p. 1-13.
6. Carretta, Y., A. Hunter, R. Boman, J.-P. Ponthot, N. Legrand, M. Laugier, and R. Dwyer-Joyce, *Ultrasonic roll bite measurements in cold rolling: Contact length and strip thickness.* Proceedings of the Institution of Mechanical Engineers, Part J: Journal of Engineering Tribology, 2018. **232**(2): p. 179-192.
7. Lowe, M.J., *Matrix techniques for modeling ultrasonic waves in multilayered media.* IEEE transactions on ultrasonics, ferroelectrics, and frequency control, 1995. **42**(4): p. 525-542.
8. Pilarski, A. and J. Rose, *Ultrasonic oblique incidence for improved sensitivity in interface weakness determination.* NDT International, 1988. **21**(4): p. 241-246.
9. Pilarski, A., J. Rose, and K. Balasubramaniam, *The angular and frequency characteristics of reflectivity from a solid layer embedded between two solids with imperfect boundary conditions.* The Journal of the Acoustical Society of America, 1990. **87**(2): p. 532-542.
10. Pialucha, T., M. Lowe, and P. Cawley, *Validity of different models of interfaces in adhesion and diffusion bonded joints*, in *Review of Progress in Quantitative Nondestructive Evaluation*. 1993, Springer. p. 1547-1554.
11. Liaptsis, D., B.W. Drinkwater, and R. Thomas, *The interaction of oblique incidence ultrasound with rough, partially contacting interfaces.* Nondestructive Testing and Evaluation, 2006. **21**(3-4): p. 109-121.
12. Nam, T., T. Lee, C. Kim, K.-Y. Jhang, and N. Kim, *Harmonic generation of an obliquely incident ultrasonic wave in solid–solid contact interfaces.* Ultrasonics, 2012. **52**(6): p. 778-783.
13. Kendall, K. and D. Tabor, *Ultrasonic Study of Area of Contact between Stationary and Sliding Surfaces.* Proceedings of the Royal Society of London Series a-Mathematical and Physical Sciences, 1971. **323**(1554): p. 321-340.
14. Thomas, T.R. and R.S. Sayles, *Stiffness of machine tool joints: Arandom-process approach.* Journal of Engineering for Industry, 1977: p. 99:250.
15. Dwyer-Joyce, R.S., P. Harper, and B.W. Drinkwater, *A method for the measurement of hydrodynamic oil films using ultrasonic reflection.* Tribology Letters, 2004. **17**: p. 337-48.
16. Pialucha, T.P., *The reflection coefficient from interface layers in NDT of adhesive joints*. 1992, Doctoral Thesis, University of London.
17. Sharma, K. and R.R. Bhargava, *Propagation of thermoelastic plane waves at an imperfect boundary of thermal conducting viscous liquid/generalized thermoelastic solid.* Afrika Matematika, 2014: p. 1-22.
18. Rokhlin, S. and Y. Wang, *Analysis of boundary conditions for elastic wave interaction with an interface between two solids.* The Journal of the Acoustical Society of America, 1991. **89**(2): p. 503-515.
19. Rokhlin, S. and D. Marom, *Study of adhesive bonds using low-frequency obliquely incident ultrasonic waves.* The Journal of the Acoustical Society of America, 1986. **80**(2): p. 585-590.